Equilibrium and Stability of High-Beta Plasmas in Wendelstein 7-AS

M.C. Zarnstorff[1], A. Weller[2], J. Geiger[2], E. Fredrickson[1], S. Hudson[1], J. Knauer[2], A. Reiman[1], A. Dinklage[2], G.-Y. Fu[1], L.P. Ku[1], D. Monticello[1], C. Nührenberg[2], A. Werner[2], the W7-AS Team and NBI-Group.

[1]*Princeton Plasma Physics Laboratory, Princeton, NJ 08543 USA*
[2]*Max-Planck Institute for Plasma Physics, EURATOM Assoc., D-17491 Greifswald, Germany*

e-mail contact of main author: zarnstorff@pppl.gov

Abstract. Quasi-stationary, MHD-quiescent discharges with volume averaged beta-values up to 3.4% were sustained in the W7-AS for more than 100 energy confinement times. A stability limit was not observed. The achieved beta appears to be limited by confinement, but is sensitive to the magnetic configuration. The decrease in beta for vacuum rotational transform < 0.5 is consistent with an equilibrium beta-limit given by a Shafranov axis-shift of one-half the minor radius. The plasma equilibrium is reconstructed, fitting the magnetic diagnostic measurements and the Thomson-scattering pressure profile, using a modified version of the STELLOPT. Analysis of the free-boundary equilibria by PIES indicate that the beta-limit and its variation may be due to deterioration of the flux surfaces and generation of magnetic stochasticity. Low-frequency n =1 and 2 MHD activity is often observed at intermediate beta-values, but does not impede access to higher-beta. Linear ideal-MHD free-boundary stability calculations indicate that the plasma should be unstable for beta < 2.5%. This severely underestimates the achievable beta-values.

1. Introduction and plasma characteristics

Achieving high plasma pressure in stationary plasma conditions, without disruptive activity, is a key challenge for developing fusion energy. Quasi-stationary, quiescent discharges with volume averaged beta $\langle\beta\rangle$-values up to 3.5% were achieved in the five-period Wendelstein 7-AS stellarator [1]. The processes that limit the accessible β values are investigated to develop an understanding of 3D stability and the expected operating limits for new experiments.

The highest β values in W7-AS were obtained at low magnetic field B=0.9 – 1.1 T and a vacuum rotational transform $\iota_{ext} \sim 0.5$. A typical example is shown in Fig. 1, where a $\langle\beta\rangle$ = 3.4% plasma is maintained in steady conditions, heated by 3.9 MW of co-tangential hydrogen neutral beam injection into a hydrogen plasma. The total plasma current was feedback controlled to be approximately zero, using an Ohmic current to cancel the net bootstrap and beam-driven current. The line-averaged electron density $\bar{n}_e \sim 2\times10^{20}$ m^{-3} and the plasma has the characteristics of the HDH enhanced confinement regime [2]. These high-β plasmas were only obtained after the island divertor structures were installed. However, the divertor control coils are energized to suppress edge islands and maximize the plasma volume, so an island divertor edge configuration is not expected.

During the high-β phase, the plasma is typically quiescent and large-scale MHD activity is not apparent. The plasma pressure was maintained as long as the heating power was supplied or until the power handling capability of the plasma-facing components was exceeded, leading to an uncontrolled increase in radiated power and loss of stored energy. As shown in Figure 2, the maximum β was approximately independent of pulse length and was maintained for more than 100 energy confinement times. A stability limit was not observed, and the maximum beta was not limited by the onset of observable instabilities. The

β apparently was limited by confinement and heating power, but was also sensitive to the magnetic configuration. W7-AS had a flexible coil set, with toroidal field coils for varying the rotational transform ι, special modular coils for varying the toroidal mirror ratio, island-divertor control coils, and vertical field coils in addition to the main modular coils. All of these modify the magnetic configuration and affect the achieved β.

Figure 3 shows the variation of β with the divertor control-coil current, I_{CC}. The control-coils were designed to make a resonant magnetic perturbation for control of edge islands, and are calculated to have no effect on ι or on the neoclassical ripple transport in the collisionless regime. Yet, they strongly affect the quiescent β value, in plasmas showing no strong MHD activity. Similarly, for $\iota_{ext} < 0.5$, the calculated Shafranov shift of the magnetic axis approaches <a>/2, where <a> is the average minor radius, and β appears to be constrained by the classical equilibrium limit. Thus, there are strong indications that characteristics of the plasma equilibrium control the accessible β.

2. Equilibrium reconstruction

An accurate reconstruction of the plasma equilibrium is needed to understand these high-β plasmas and compare them to theoretical models. This includes a determination of the profiles of the plasma pressure and ι, including the effect of plasma currents. The data readily available on W7-AS includes a 45-point Thomson scattering system and 19 magnetic diagnostics (two diamagnetic loops at different toroidal positions and orientations, a Rogowski loop, a 4-segment Rogowski array, and 12 saddle loops of 3 shapes). The time-integration of the magnetic diagnostics starts after the magnetic fields reach their programmed values, and they are compensated for residual noise variations of the field coil currents. Thus, the diagnostics only measure the plasma-induced signal. The uncertainty of the magnetic measurements is estimated to be ±3%, mainly due to uncertainties in location and shape. The electron pressure profile shape measured by Thomson scattering characterizes the total pressure profile shape, as that the ion and electron temperatures are strongly equilibrated due to the high plasma density, $n_e(0) > 10^{20}$ cm^{-3}. The non-thermal beam stored energy is estimated to be less than 5% of the total plasma energy.

The stellarator design-optimization code STELLOPT [4] has been modified to reconstruct the W7-AS equilibrium self-consistently. STELLOPT uses the free-boundary inverse-equilibrium solver VMEC [5] to calculate the 3D plasma equilibrium given specified coil currents and plasma pressure and current profiles, which are represented as polynomials in the normalized toroidal flux. VMEC assumes that the equilibrium has nested toroidal flux-surfaces. An improved Levenberg-Marquardt search is used to adjust the profiles or other free parameters to minimize the deviation of specified criteria with specified weights. To serve as a reconstruction code, STELLOPT was modified to target the experimental conditions, thus providing a least-squares fit to the available diagnostics. The modifications include: (1) Adjusting the plasma size to minimize the separation between the plasma surface and a set of piecewise-linear limiting surfaces at specified toroidal angles, representing the many in-vessel structures present in the experiment. (2) Adjusting the pressure polynomial coefficients to match the set of pressure data points measured by Thomson scattering. Only the shape of the measured profile is used, the amplitude is adjusted to match the magnetic diagnostics, or the diamagnetic stored energy (if not fitting to magnetic measurements directly). (3) Adjusting the current and pressure polynomial coefficients to match the set of magnetic diagnostic measurements with simulations calculated by the

DIAGNO code [6] based on the VMEC equilibrium solution. The weights for the fit are set to be the inverse of the one-standard-deviation uncertainty for each measurement.

STELLOPT iterates the fit using fully-converged VMEC equilibrium solutions. Thus, this technique is computationally expensive compared to tokamak equilibrium reconstruction codes, or the approach being implemented in the V3FIT project [7,8]. A typical analysis requires 2-3 hours on a 16-CPU cluster. However, the computation inefficiency is balanced by the ease of incorporating additional diagnostics and the extensive set of theoretical models already available from the design-optimization studies.

The information content of the magnetic diagnostics has been investigated by principal component analysis of a database of simulated equilibria using methodically varied profiles, but no total toroidal current. An earlier analysis [9] of the W7-AS magnetic diagnostics found six significant principal components, but did not attempt to distinguish between profile and magnetic configuration information. All the magnetic diagnostics respond strongly to the plasma energy. The diagnostic response for fixed plasma energy and coil currents was analyzed, finding two significant empirical orthogonal functions (EOF) together accounting for 99.9% of the variance due to variations of the pressure profile shape. There is only one EOF that accounts for all the variance due to changes of the current profile shape (for no total current). The EOF coefficients depend on the plasma energy analyzed, which may be due to the non-linear character of the equilibrium equation. Due to finite measurement uncertainty, the sensitivity to the pressure and current profiles are linked. Thus, independent measurements of the pressure profile are needed to constrain the current profile fit.

Figure 4 shows the pressure profile for the β=3.4% plasma of Figure 1, from the fit to the Thomson scattering and magnetic diagnostic measurements. The pressure profile was fit by a 10-term polynomial, with an 11^{th} term used to constrain the edge pressure to zero. The Thomson scattering measurements show considerable scatter beyond their calculated uncertainty, leading to a χ^2_{TS} of approximately 3 per Thomson data point. The largest single contribution is from the single-point discrepancy at R=2.11m. Other plasmas have been fit with a χ^2_{TS} as low as ~ 1.5 per Thomson data point. The total plasma energy from the fitted pressure profile agrees with the diamagnetic loop energy analysis, with a difference of ~2%. The edge pressure pedestal in Fig. 4 is present in many but not all high-β plasmas.

The current profile, shown in Fig. 5, was fit using a 3-term polynomial, since the magnetic diagnostics are only sensitive to one current profile shape EOF and the total current. Fourth and tenth-order terms were used to force the current to go to zero at the edge. Sensitivity calculations show that the diagnostics cannot distinguish between profiles with finite edge current density or constrained to have no edge current density. In either case, the resulting χ^2_{mag} for the magnetic diagnostic is ~ 0.83 per measurement. Equilibrium fits varying 4 moments did not lower χ^2 or change the appearance of the current profile. Use of 5 or more moments led to solutions with large alternating-sign coefficients and large radial oscillations in the current and ι profiles, indicating over-fitting. Figure 5 also shows a comparison between the fitted current profile and kinetic calculations [10] of the net current profile from the competing beam, bootstrap, and Ohmic currents, for two different Z_{eff} profile assumptions. The fitted current profile is approximately three-times larger than the calculated net current profile in the outer region. Imposing the calculated current profiles

increases χ^2_{mag} by a factor of 1.8 – 2.4, thus they appear to be inconsistent with the magnetic measurements. The sensitivity of the magnetic diagnostics to the magnitude of the current profile is mainly through sensor coils 3 and 4 of the segmented Rogowski array, and saddle-loop 1 (to a lesser extent). The sensitivity of these measurements to changes in the magnitude of the current profile is shown in Fig. 6, which indicates that the uncertainty in the magnitude of the current profile is approximately ±20%. Thus, while the inferred currents are small, the difference between the calculated and fit current profiles is significant.

3. Equilibrium topology

The large Shafranov shift of the magnetic axis, nearing a/2, and the sensitivity of the achieved β to the magnetic configuration, suggests that the plasma confinement and β may be influenced by details of the equilibrium, including the formation of islands and stochastic regions. To assess this, the dependence of the plasma β on the control coil current has been studied using the PIES code [11], which does not assume closed flux-surfaces. Free-boundary three-dimensional equilibria have been numerically calculated for the plasmas of Fig. 4, scanning only I_{CC}. The calculations use the pressure profile from the equilibrium reconstruction, as discussed above. $\langle\beta\rangle \sim 2.7\%$ was achieved with the optimum control-coil current ($I_{CC} = -2.5$ kA), but this fell to $\langle\beta\rangle \sim 1.8\%$ for $I_{CC} = 0$. The PIES calculated equilibria for these cases indicate that the outer ~ 35% of the flux surfaces are stochastic in both plasmas at their (different) $\langle\beta\rangle$ values, see Fig. 7. Radial transport in the stochastic region may be enhanced due to transport parallel to the magnetic field, limiting the ability to access higher β. PIES equilibria were calculated as a function of $\langle\beta\rangle$, keeping the pressure profile shape fixed. Figure 8 shows that the calculated fraction of good flux surfaces drops with increasing β for all cases, but the drop occurs at higher β for $I_{CC} = -2.5$ kA than for $I_{CC} = 0$. In both cases, the fraction of good flux surfaces plunges slightly above the achieved $\langle\beta\rangle$. Thus, the PIES equilibria indicate that the experimental β limit and its variation due to the control coil current may be due to deterioration of the flux surfaces and the effect of magnetic stochasticity on the plasma confinement.

The 3.4% plasma shown in Fig. 1 was obtained with I_{CC}=-2.95 kA but a lower magnetic field (0.9 T) than the plasmas in Fig. 4. Thus, the perturbation made by the control coil was ~40% stronger. The equilibrium for this case is being analyzed by PIES.

The PIES equilibrium calculations can also attempt to simulate the response of the plasma to changes in the flux surface topology by flattening the plasma pressure in any region calculated to have stochastic field lines or be inside an island. In this case, the non-linear evolution of the calculation progressively shrinks the plasma, so that the calculated equilibrium is fully stochastic and there is no pressure gradient for initial $\langle\beta\rangle \geq 1\%$ ($I_{CC} = 0$) or $\geq 2\%$ ($I_{CC} = -2.5$kA). The disagreement between these collapsed equilibrium calculations and the observed plasmas with higher $\langle\beta\rangle$ indicates that a more sophisticated plasma response model is required [12]

4. MHD stability – low mode number

Low-frequency MHD activity with poloidal mode number $m \leq 5$ is often observed for $1.5\% < \beta < 2.5\%$, during the increase in β after the increase of beam power. These modes saturate without impeding access to higher-β values, and do not degrade confinement in most cases..

Linear ideal-MHD free-boundary stability calculations using CAS3D [13] for a plasma with $\iota_{ext} = 0.52$, assuming a parabolic pressure profile, indicate that the m/n = 2/1 mode should be unstable for $\langle\beta\rangle < 2.5\%$ [14, 3], where n is the toroidal mode number. The observed MHD activity is consistent with these stability calculations. These calculations have been confirmed for the reconstructed pressure profile of the plasma in Fig. 1 using the Terpsichore [15] linear-stability code,. Scaling the high-beta pressure profile to lower-β values, the m/n=2/1 mode is calculated to be unstable for $1\% \le \langle\beta\rangle \le 2.5\%$. The m/n=2/1 stability is controlled by changes in the ι profile and the calculated stability for $\langle\beta\rangle > 2.5\%$ is due to ι moving away from 0.5 in the calculated equilibrium. Since the observed instability saturates and does not limit access to higher $\langle\beta\rangle$ values, the low-n ideal-MHD linear stability threshold significantly underestimates the achievable β.

The dependence of the MHD stability on ι was investigated during the heating flat-top to avoid the evolving pressure and iota profiles that may be present during the initial increase of β. The variation of β and MHD activity during a detailed ι_{ext} scan is shown in Figure 9. Significant MHD instabilities are observed only in very narrow regions of ι_{ext}. No disruptions were observed, in all cases the MHD activity saturated and the plasma continued. For the plasma with ι_{ext} ~0.51, arrays of external Mirnov coils observe a small saturated oscillation at 4.9 kHz with m=2. In some of the plasmas, higher frequency oscillations are also detected with m=0 or m=1. For the plasmas with stronger MHD activity at ι_{ext} ~0.53 and ι_{ext} ~0.59, the mode number could not be unambiguously determined. The flattop $\langle\beta\rangle$ varies smoothly with ι_{ext}, except in the plasmas with large-amplitude MHD activity. The difference between a configuration with large MHD instabilities and a neighboring stable one is due to a ~ 4% change in the toroidal-field coil current and a compensating <1% change in the modular coil current. Thus, the stability of the plasma was easily controlled using the external coils.

5. MHD stability – high mode number

The high beta plasmas discussed so far are calculated to be stable to high-n ballooning instabilities using the COBRA code [16]. For the bulk of the plasma profile, there are no nearby stability thresholds calculated, thus ballooning modes are not expected to limit the plasma β**.** High mode-number instabilities are not observed, as long as the electron temperature is kept high enough to avoid resistive instabilities[14].

In W7-AS, the magnetic field ripple or toroidal mirror depth can be varied by changing the current in the 'corner' modular coil ('I_5'). This also increases the vacuum magnetic hill, though finite plasma pressure generates a net magnetic well. Experiments with $I_5 > I_M$ showed a bifurcated behavior, see Fig. 10. At the onset of neutral beam heating, frequent fast MHD bursts were observed and the plasma β was limited to ~0.6% for a prolonged period. Suddenly, the MHD bursts ceased and the β increased to ~2.7% similar to the standard configuration. The duration of the bursting period increased with increasing magnetic mirror ratio. Linear stability calculations of the ideal localized ballooning mode, using COBRA, indicated that the high β-phase appeared to be in the second-stability regime. This prompted an investigation of the evolution of the ballooning threshold during the increase in plasma pressure, to understand how the second-stable regime was accessed. Figure 11 shows stability diagrams [17] for a sequence of free-boundary equilibria with increasing β from left to right for the r/<a>=0.7 (half flux) surface. The dotted line shows

the stability boundary for the symmetric field line passing through θ=0, φ=0, and the solid line shows the stability boundary envelope for the whole flux surface. The measured pressure profile is calculated to be in the second stable region inside of r/a ~ 0.8. From the calculated sequence of boundaries versus β, it appears that the plasma accesses this region along a stable trajectory, due to an increase of shear with plasma pressure and a deformation of the stability boundary.

5. Summary

Quiescent quasi-steady plasmas with ⟨β⟩ up to 3.5% were achieved in W7-AS, and maintained for more than 100 energy confinement times. There was no indication of a stability pressure limit, rather the achieved β appeared to be limited by energy confinement and heating power. The plasma equilibrium was reconstructed fitting external magnetic measurements and Thomson scattering measurement of the electron pressure profile. PIES calculations of the equilibrium indicates that a stochastic-field region forms at the edge of the plasma as β increases, and that the observed saturated ⟨β⟩ values correspond to a loss of approximately 35% of the flux. An abrupt loss of flux-surface integrity is predicted for β values above those observed. Thus, the onset of stochastic magnetic fields and the loss of good flux surfaces may control the transport and achievable ⟨β⟩ value. This result is favourable for the new stellarators NCSX and W7-X, which were designed to maintain good flux-surfaces at high-β.

These plasmas often experience m/n=2/1 instabilities at intermediate ⟨β⟩ < 2.5%, in reasonable agreement with linear instability calculations indicating a threshold of ⟨β⟩~1%. However, the instability saturates and does not inhibit access to high β values. Thus, the linear stability threshold is not a good indication of the β-limit. Strong MHD instabilities only observed in very narrow ranges of ι_{ext} and can be avoided by small changes in the coil currents.

Acknowledgement

We are grateful for the support and encouragement of Prof. T. Klinger, Prof. R. Goldston, and Dr. R. Nazikian. We would like to thank Dr. S.P. Hirshman, Dr. W.A. Houlberg, and Dr. A. Cooper for providing the VMEC, AJAX, and TERPSICHORE codes, respectively. This work was supported by U.S. DoE Contract DE-AC02-76-CHO-3073.

Figures:

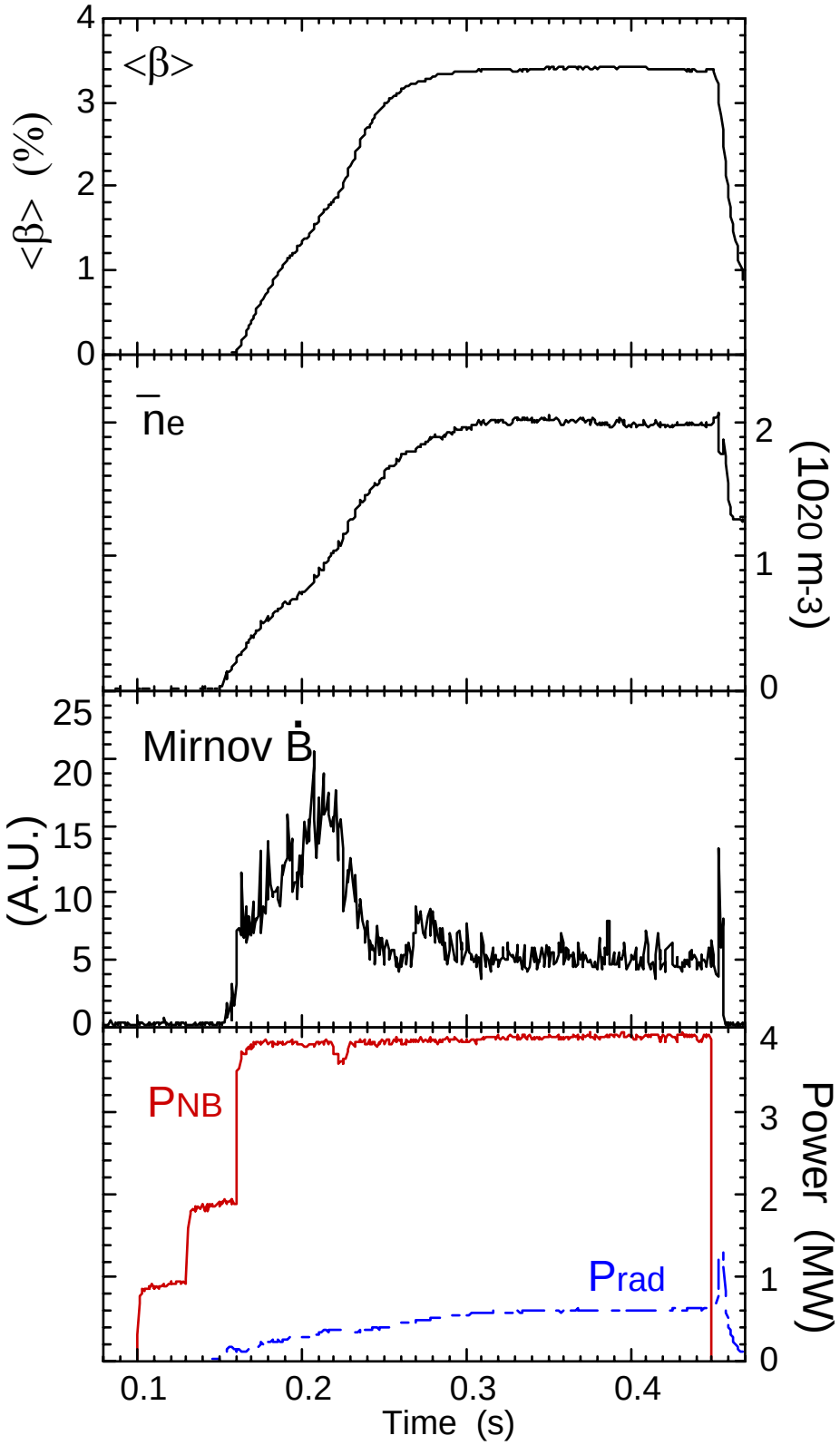

Figure 1.Time evolution of a quasi-stationary, quiescent plasma with ⟨β⟩ = 3.4%, B = 0.9T, P_{NB}=3.9 MW, $\iota_{ext}(0)$ = 0.47, and I_{CC} = 2.96 kA.

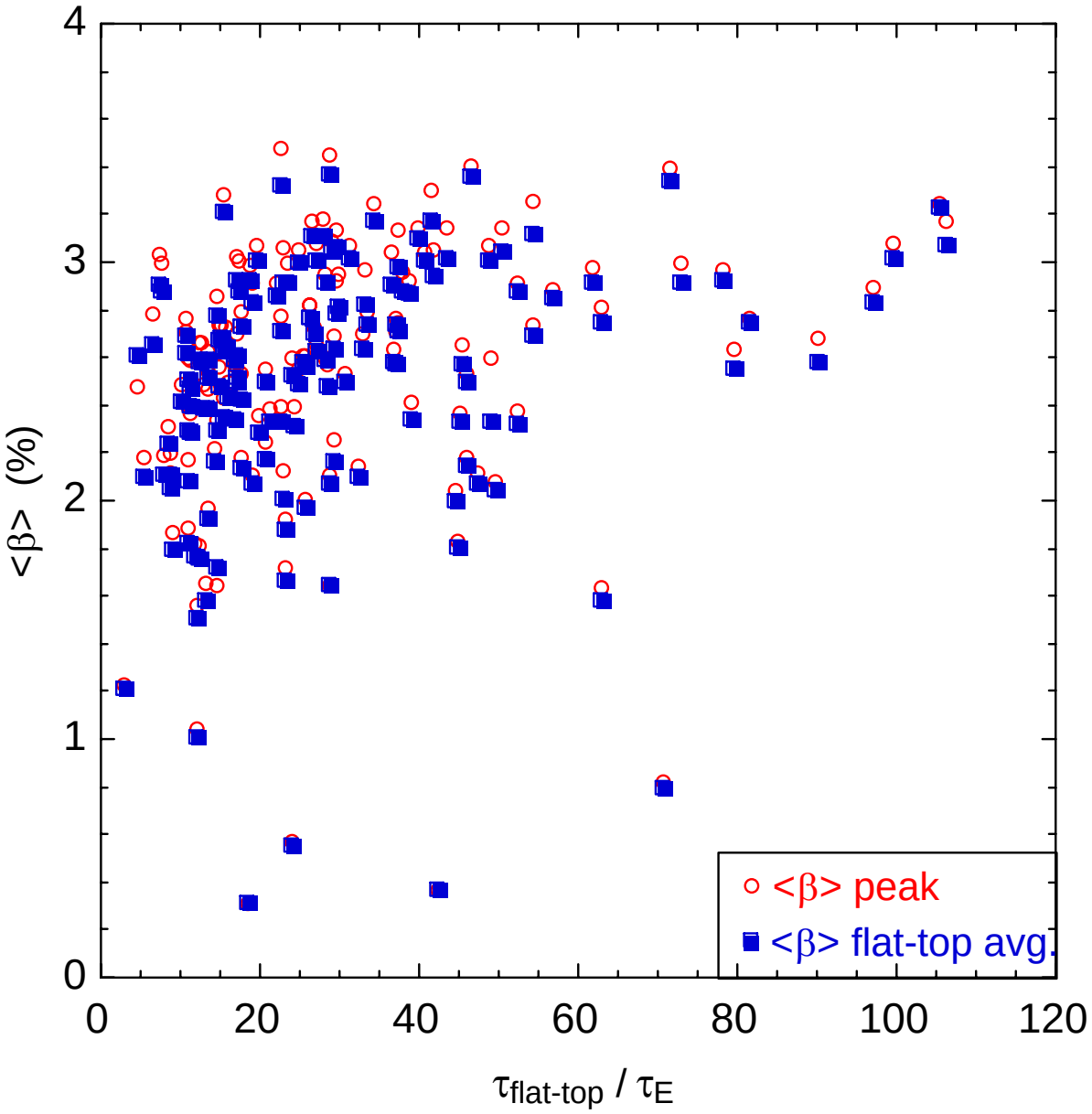

Figure 2. Database plot showing ⟨β⟩ versus the sustained time-duration divided by the energy confinement time. The open symbols give the peak-⟨β⟩ value, and the closed symbols are the time-average value. The small difference between the symbols is an indication of the steady plasma conditions.

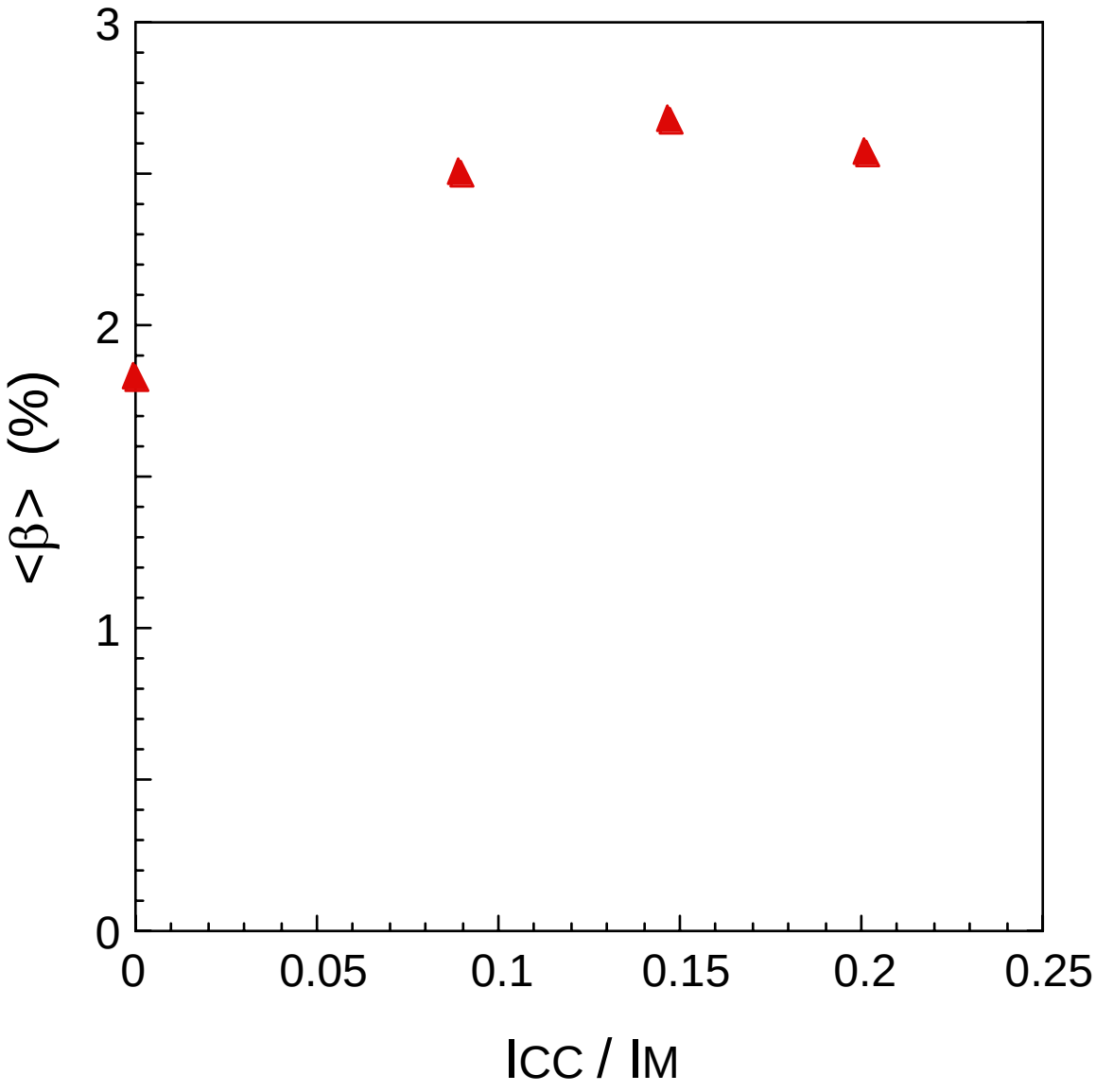

Figure 3. Variation of peak-⟨β⟩ versus the divertor control-coil current I_{CC} normalized by the modular coil current, for B=1.25 T, P_{NB} = 3.4 MW and ι_{ext} = 0.44.

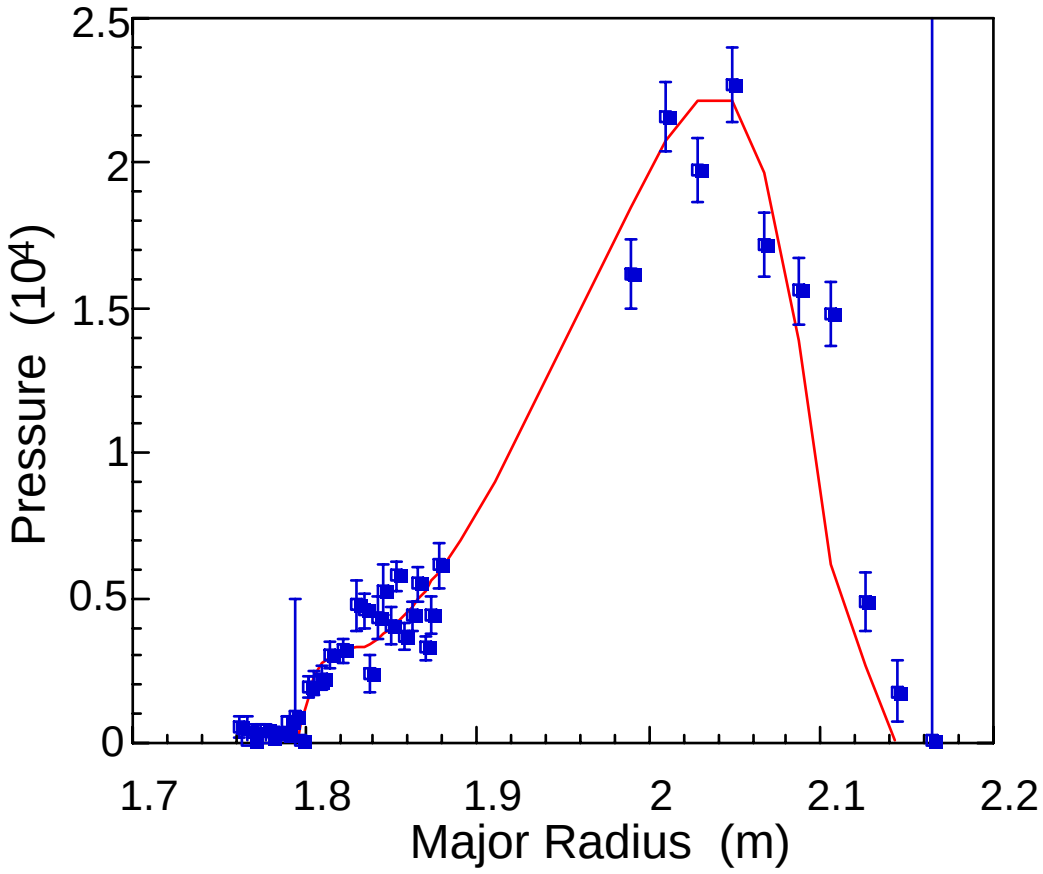

Figure 4. For the plasma of Figure 1, measured pressure profile (points) from Thomson scattering and fit profile from reconstruction (line). The data points are twice the measured electron pressure.

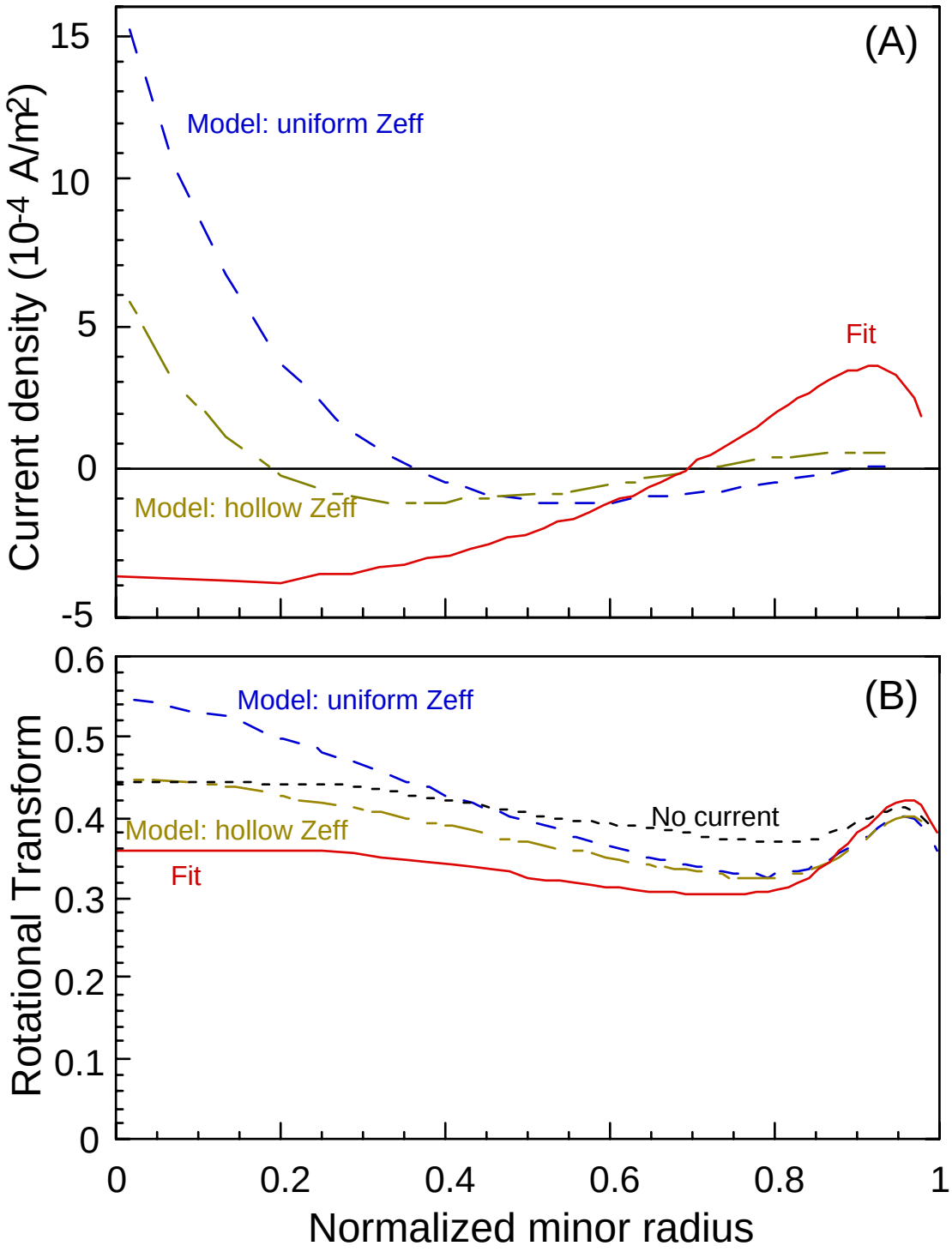

Figure 5. (A) Current profiles from equilibrium fit (solid) compared with kinetic current calculations using either uniform Zeff (dashed) or a hollow Zeff profile (dot-dashed) . (B) Rotational transform profile from equilibrium fitting (solid) compared with equilibria calculated with kinetic calculations (dashed and dot-dashed) or assuming no net toroidal current density (short-dashed).

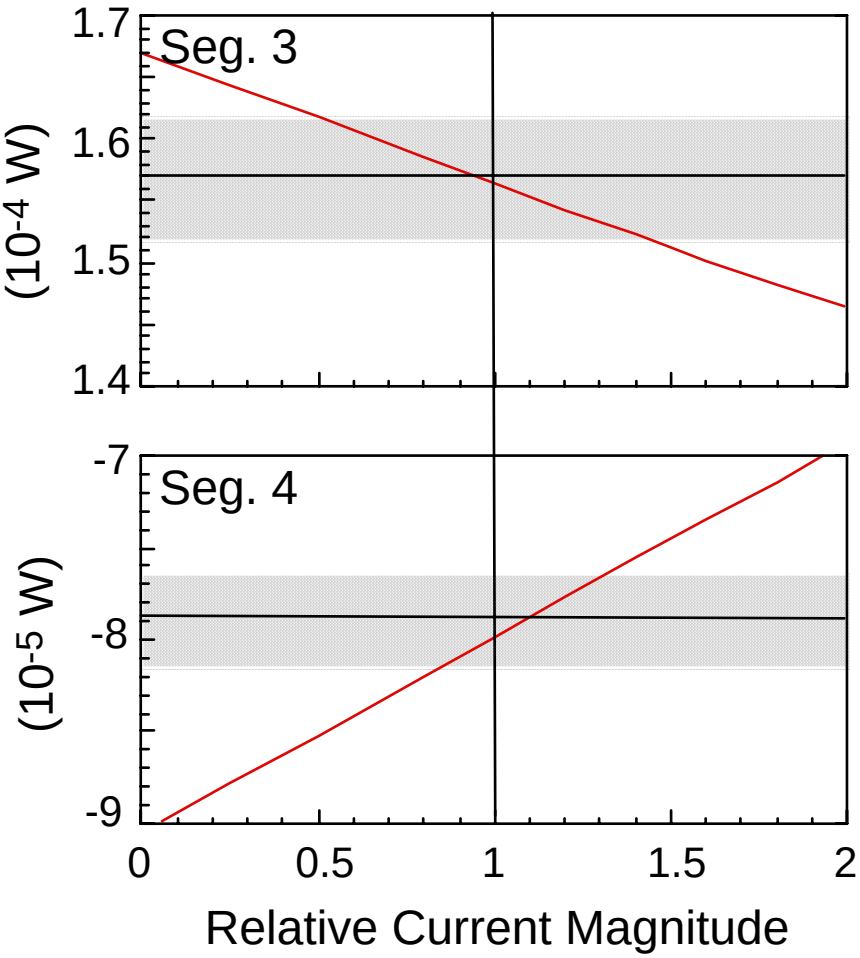

Figure 6. Simulated signals for segmented Rogowski-array sensor coils 3 (A) and 4 (B) versus the relative magnitude of the plasma current profile, where 1 represents the fitted current in Fig. 5. Also shown are the measured values (horizontal lines) and the range of uncertainty (shaded bands).

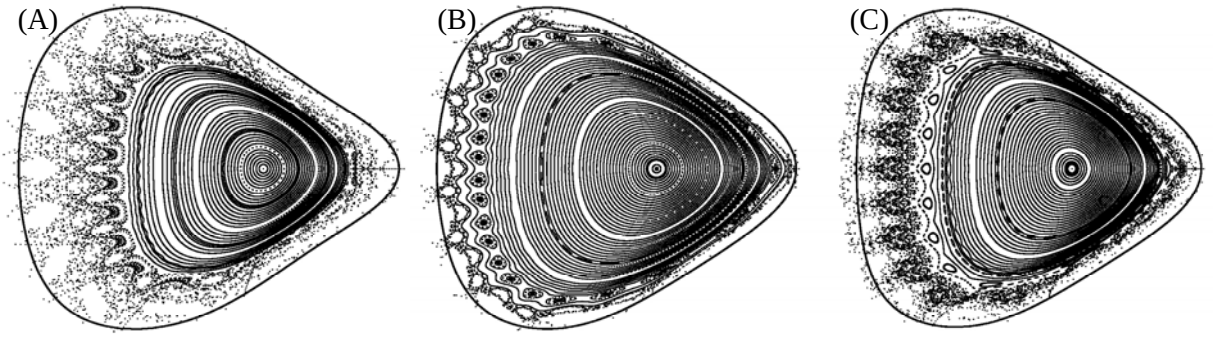

Figure 7. PIES calculated flux surface topologies at the triangular symmetry plane for two of the plasmas in Fig. 4: (A) I_{CC}=0 and $\langle\beta\rangle$ = 1.8%, (B) I_{CC}=-2.5kA and $\langle\beta\rangle$ = 2.0%, (C) I_{CC}=-2.5kA and $\langle\beta\rangle$ = 2.7%. In each case, the dark line is the STELLOPT/VMEC calculated plasma boundary.

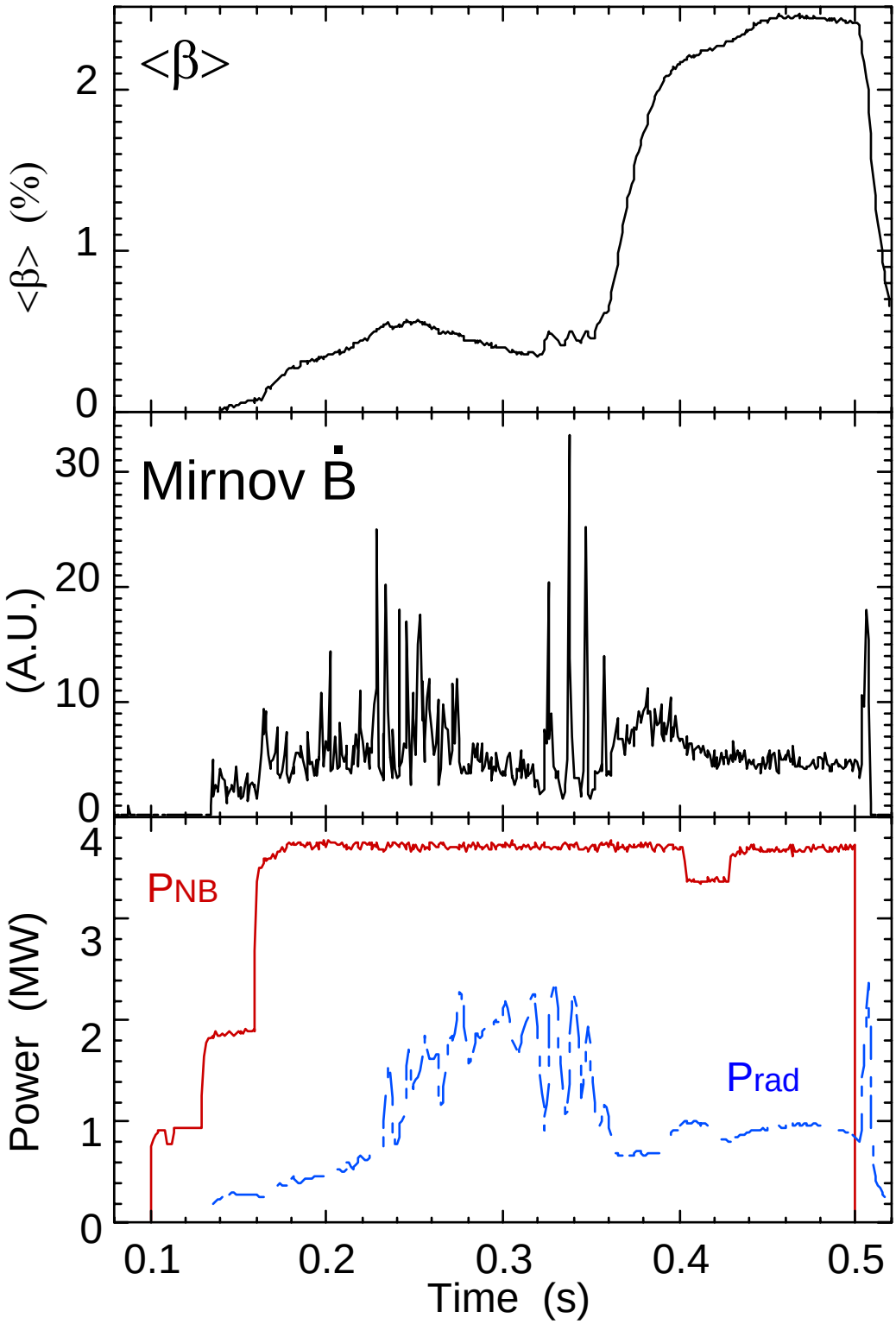
<β>
<β> (%)
2
1
0
Mirnov Ḃ
(A.U.)
30
20
10
0
PNB
Prad
Power (MW)
4
3
2
1
0
0.1
0.2
0.3
0.4
0.5
Time (s)

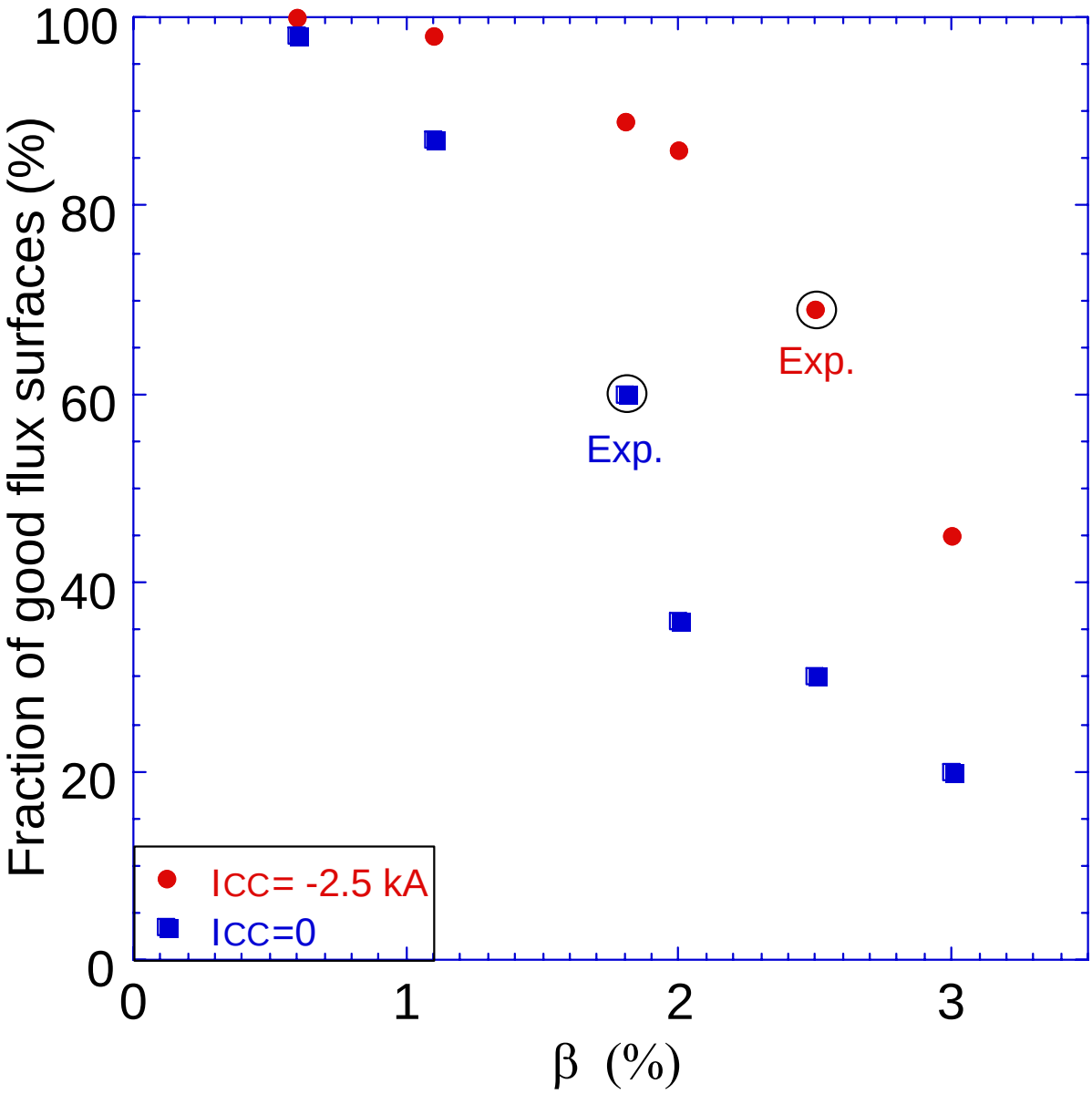

Figure 8. Fraction of good flux surfaces versus ⟨β⟩ for two plasmas of Fig. 4: I_{CC}=0 and I_{CC}=-2.5kA

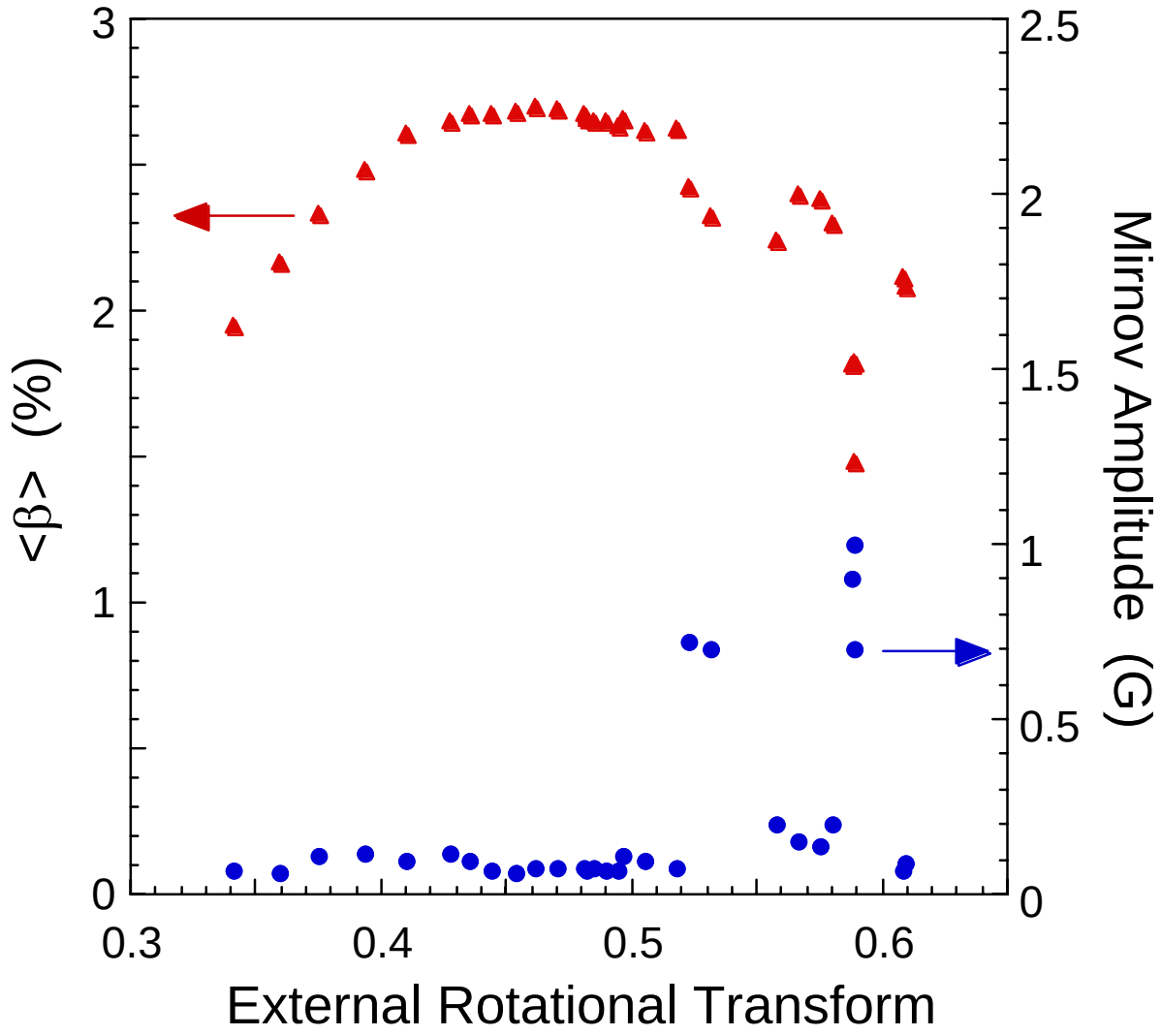

Figure 9. Variation of ⟨β⟩ (left scale) and the amplitude of $\dot{B}$ fluctuations (right scale) versus the external rotational transform ι_{ext} during the heating flat-top for B=1.25 T, P_{NB} = 3.4 MW, and I_{CC} = 2.5 kA.

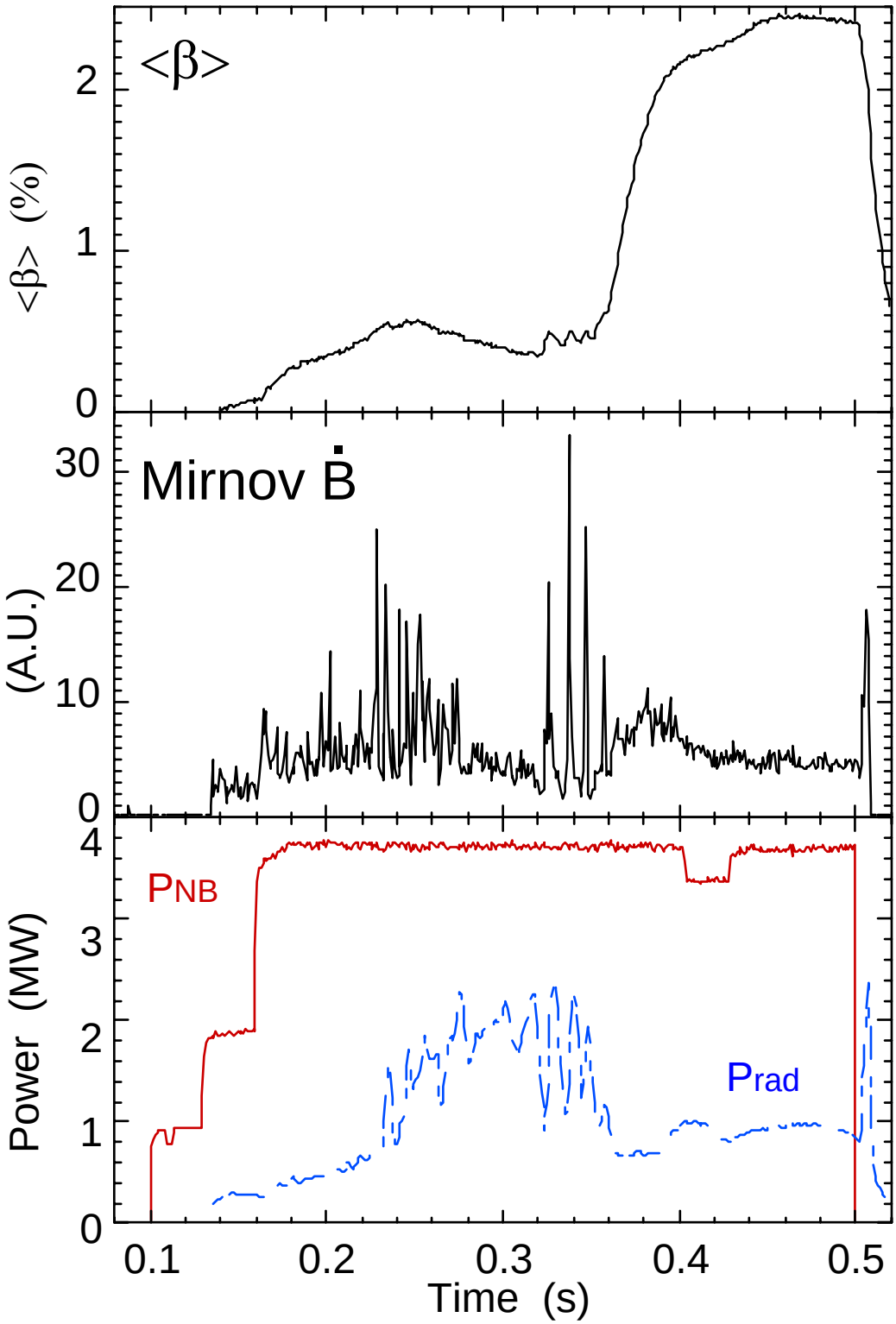

Figure 10. Time evolution of ⟨β⟩ and Mirnov signal for a plasma with I_5/I_M = 1.3, showing initial unstable period followed by a transition to high-β.

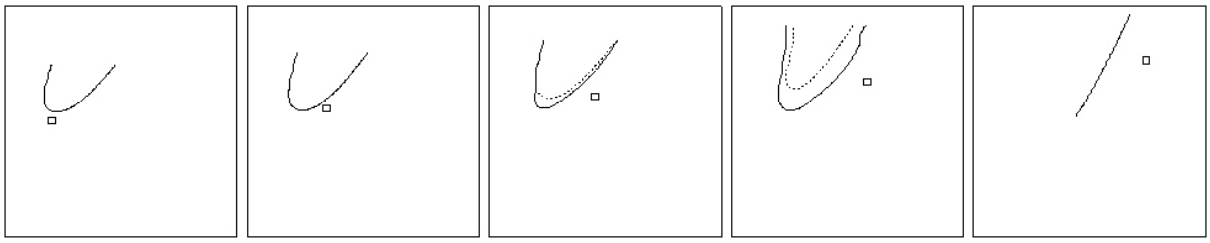

Figure 11. Stability diagrams for the configuration of the plasma showing in Fig. 10, for r/a = 0.7 and (a) $\langle\beta\rangle$ = 0.5%, (b) $\langle\beta\rangle$ = 1.0%, (c) $\langle\beta\rangle$ = 1.5%, (d) $\langle\beta\rangle$ = 2.0%, (e) $\langle\beta\rangle$ = 2.5%.. In each diagram, ι' is plotted versus p'. The symbols indicate the measured value and the curve indicates the stability boundary for the flux-surface. The dashed curve indicates the stability boundary for the θ=0, φ=0 field-line.

References

[1] A. Weller et al, IAEA Nuclear Fusion and Plasma Phys. 2002 (Lyon), paper EX/S3-1.
[2] K. McCormick et al., Phys. Rev. Lett. **89** (2002) 015001.
[3] J. Geiger et al., Fusion Sci. and Technology **46** (2004) 13.
[4] D. Strickler et al, IAEA Nuclear Fusion and Plasma Phys. 2002 (Lyon), paper FT/P2-06.
[5] S.P. Hirshman et al., Comput. Phys. Commun. **43** (1986) 143.
[6] H.J. Gardner, Nucl. Fusion **8** (1990) 1417.
[7] S.P. Hirshman et al., Phys. Plasmas **11** (2004) 595.
[8] N. Pomphrey et al, this conference, paper IC/P6-45.
[9] H.P. Callaghan, et al., 25th EPS Conf. on Contr. Fusion and Plasma Phys., Praha, ECA Vol. **22C** (1998) 1470.
[10] J. Geiger et al, 30th EPS Conf. on Contr. Fusion and Plasma Phys., St. Petersburg, ECA Vol. **27A** (2003) 1470.
[11] A.H. Reiman and H. Greenside, Compt. Phys. Commun. **43** (1986) 157.
[12] A.H. Reiman et al, this conference, paper IC/P6-46.
[13] C. Nührenberg, Phys. Plasmas **6** (1999) 137.
[14] A. Weller et al., Plasma Phys. Control. Fusion **45** (2003) A285.
[15] D.V. Anderson et al, Scient. Comp. Supercomputer **II** (1990) 159.
[16] R. Sanchez et al., J. Comput. Phys. **161** (2000) 589.
[17] S.R.Hudson and C.C.Hegna. Physics of Plasmas **10** (2003):4716.